Article

Discovery Medicine 2026; 38(207): 1180–1194
https://doi.org/10.24976/Discov.Med.202638207.94

Notoginsenoside R1 Restores Endothelial Progenitor Cells Function to Relieve Atherosclerosis by Inhibiting STAT3-Mediated HPSE Transcription

Fang Fang[1,2,*]

[1]Department of Traditional Chinese Medicine, Shaoxing People's Hospital, 312000 Shaoxing, Zhejiang, China
[2]School of Medicine, Shaoxing University, 312000 Shaoxing, Zhejiang, China
*Correspondence: fangfangtj@126.com (Fang Fang)
Submitted: 10 December 2025 Revised: 14 January 2026 Accepted: 3 February 2026 Published: 20 April 2026

Background: Endothelial progenitor cells (EPCs) can alleviate atherosclerosis (AS) through their roles in endothelial repair and angiogenesis, but their function is often impaired under pathological conditions. Notoginsenoside R1 (NGR1), an extract from traditional Chinese medicine, has demonstrated therapeutic efficacy in alleviating AS. This study aims to investigate whether NGR1 ameliorates AS progression by restoring EPCs' dysfunction.

Methods: Apolipoprotein E-deficient (ApoE$^{-/-}$) mice were treated with angiotensin II for 4 weeks to establish an AS model, and treated with long-term infusion of NGR1 using an Alzet osmotic micropump. Metabolic characteristics and pathological changes in aortic tissues were measured using kits, Hematoxylin and Eosin (H&E) staining, Masson staining and Oil red O staining. EPCs extracted from mice were verified by immunofluorescence staining and then were treated with NGR1, Signal transducer and activator of transcription 3 (STAT3) overexpression plasmid (oe-STAT3) and / or Heparanase short hairpin RNA (shHPSE). The biological behaviors of EPCs were determined using cell counting kit 8, colony formation, scratch assay and tube formation assay. The relationship between STAT3 and HPSE was determined by Dual-luciferase reporter assay and Chromatin immunoprecipitation. The expression levels of STAT3, HPSE and syndecan-1 (SDC-1) were analyzed using Western blot and quantitative reverse transcription polymerase chain reaction (qRT-PCR) analyses.

Results: *In vivo*, NGR1 ameliorated disturbances of lipid metabolism and reduced aortic plaque formation in AS mice. *In vitro*, NGR1 facilitated the viability, proliferation, migration and tube formation of EPCs, while downregulating the expression levels of STAT3 and Heparanase and upregulating the SDC-1 expression level. However, these effects were reversed by oe-STAT3. STAT3 activated HPSE transcription, and the effects of oe-STAT3 on EPCs were reversed by shHPSE.

Conclusion: NGR1 restores EPCs' function by regulating the STAT3/HPSE axis, thereby alleviating the development of AS.

Keywords: Notoginsenoside R1; atherosclerosis; endothelial progenitor cells; Heparanase; Signal transducer and activator of transcription 3

Introduction

Atherosclerosis (AS) is an important contributor to mortality associated with cardiovascular disease [1]. Studies have reported that the vascular endothelium protects the blood vessels from injury by maintaining the steady state of vascular structures. However, endothelial damage and dysfunction can trigger the secretion of inflammatory factors and lipid deposition, leading to the progression of AS [2]. Fortunately, endothelial progenitor cells (EPCs) are mobilized from the bone marrow into the peripheral circulation in response to endothelial injury, and these EPCs migrate to the damaged endothelial sites to promote angiogenesis and endothelial repair through paracrine mechanisms [2,3]. However, EPCs have shown decreased numbers and impaired function in some disease conditions [2,4]. Therefore, restoring EPCs' dysfunction may be a potential strategy to ameliorate AS progression.

Globally, 80% people use plant-derived products for treating or preventing diseases [5]. In China, Panax notoginseng is widely used to treat AS, and one of its pharmacological effects is to improve endothelial injury through the regulation of endothelial cell function [6]. Notoginsenoside is the main active component of Panax notoginseng, which has been proven to promote angiogenesis of EPCs [7]. Notoginsenosides comprise multiple components, among which Notoginsenoside R1 (NGR1) is considered a primary contributor to their biological activity [8]. NGR1 has a variety of pharmacological activities, including cardiovascular protection, blood glucose regulation, immune regulation, and liver protection [9]. Notably, Lei Zhang *et al*. [10] reported that NGR1 in combination with ginsenoside Rg1 and protocatechuic aldehyde could alleviate AS by improving vascular endothelial cell dysfunction. However, whether NGR1 can alleviate AS by restoring EPCs' dysfunction remains unclear.

As interferon-alpha (IFN-α) is a key contributor to AS progression [11], we analyzed the differential gene (GSE26950) of IFN-α in the treatment of EPCs, then crossed with the target of NGR1 predicted by Swisstargetprediction [12], and obtained three genes (Heparanase (*HPSE*), Histone Deacetylase 6 (*HDAC6*) and Transient Receptor Potential Cation Channel Subfamily V Member 1 (*TRPV1*)). Among them, HPSE has been demonstrated to be implicated in AS and is considered a novel target for AS therapy [13]. In addition, we have also noted that NGR1 inhibits Signal transducer and activator of transcription 3 (STAT3) expression. As a transcription factor, STAT3 can regulate the expression of many genes and thus participates in the pathogenesis of AS [14]. We predicted using JASPAR [15] that STAT3 could regulate HPSE. Therefore, we speculate that NGR1 restores EPCs' function to alleviate the development of AS by inhibiting the transcriptional regulation of STAT3 on HPSE.

Materials and Methods

Bioinformatic Prediction of Candidate Targets

To identify potential molecular targets of NGR1 relevant to EPC dysfunction, a bioinformatic screening strategy was employed. First, differentially expressed genes (DEGs) in EPCs under inflammatory stress were obtained from the publicly available Gene Expression Omnibus (GEO) dataset GSE26950. DEGs were defined with thresholds of $|\log2(\text{fold change})| > 1$ and an adjusted p-value < 0.05. Concurrently, putative protein targets of NGR1 were predicted using the Swisstargetprediction database (http://www.swisstargetprediction.ch/), based on the canonical SMILES structure of NGR1, with a probability threshold set to >0.8. The DEGs were then intersected with the list of predicted NGR1 targets.

Animals

Apolipoprotein E-deficient ($ApoE^{-/-}$) mice (n = 24, 20–23 g, 6–8-week old) provided from Hangzhou Medical College were maintained in an SPF environment. All animal-related experimental protocols were approved by Ethics Committee of Shaoxing People's Hospital for Experimental Animals Welfare (2022Z015).

After one week of acclimatization, the mice were randomly divided into three groups (n = 8 per group): (1) Control group: mice fed a normal chow diet (XTAA, Xietong Shengwu, Yangzhou, China); (2) Model group: mice fed a high-fat Western diet (containing 21% fat and 0.15% cholesterol) (XTM05-001, Xietong Shengwu, China); (3) Model+NGR1 group: mice fed the same high-fat diet and treated with NGR1. All mice were maintained for a total of 12 weeks.

At 8 weeks of high-fat diet feeding, the Model and Model+NGR1 groups underwent surgery for Angiotensin II (Ang II, HY-13948, MedChemExpress, Shanghai, China) infusion. The AS model was established as previously described [16]. We dissolved Ang II in physiological saline, and then syringe the prepared solution into an osmotic micropump (Alzet osmotic pump, model 2004, 1000 ng/kg/min) which can continuously release drugs within 28 days. Mice were anesthetized via intraperitoneal injection of 3% pentobarbital sodium at a dose of 50 mg/kg. The skin of the left posterior cervical region of the mice was incised to the level of the superficial fascia, and then a subcutaneous tunnel approximately 4 cm in length was created using hemostatic forceps. An osmotic micropump was placed under the skin, followed by wound suture. Postoperatively, buprenorphine (0.05 mg/kg) was administered subcutaneously every 8–12 hours for 48 hours for analgesia, and Penicillin was injected into the thigh to prevent infection.

Concurrently, starting from the day of pump implantation, mice in the Model+NGR1 group received daily oral gavage of NGR1 (HY-N0615, MedChemExpress, Shanghai, China) at a dose of 100 mg/kg/day (dissolved in 0.5% sodium carboxymethyl cellulose vehicle) for 4 weeks. The Model and Control groups received equivalent volumes of the vehicle.

At the end of the 12-week dietary intervention (including 4 weeks of gavage treatment), all mice were fasted for 6 hours, anesthetized via intraperitoneal injection of 3% pentobarbital sodium at a dose of 50 mg/kg, and blood samples were collected via cardiac puncture for biochemical analysis. Blood glucose levels were measured immediately using a glucose meter (Accu-chek, Roche, Rotkreuz, Switzerland) from a separate tail vein prick sample obtained prior to terminal blood collection. Aortic tissues were subsequently dissected for histopathological analysis. Deep anesthesia was induced by intraperitoneal injection of 3% pentobarbital sodium at a dose of 70 mg/kg (confirmed by absence of pedal withdrawal reflex), terminal cardiac puncture was performed, followed by aortic dissection. The mice were then euthanized by cervical dislocation, and death was confirmed by cardiac/respiratory arrest.

Biochemical Measurements

Total cholesterol (ZC-S0690, Zcbio, Shanghai, China), Triglycerides (ZC-S0411, Zcbio, Shanghai, China), high-density lipoprotein cholesterol (HDL-C, ZC-38176, Zcbio, Shanghai, China) and low-density lipoprotein cholesterol (LDL-C, ZC-38098, Zcbio, Shanghai, China) were determined with corresponding kit according to the manufacturer's protocols.

Histopathological Examination

Aortic tissues were fixed in formalin overnight, embedded in paraffin the next day, and sectioned at a thickness of 4 µm. Paraffin sections were deparaffinized in xylene, rehydrated through a graded ethanol series (100%–90%–80%–70%) and rinsed in distilled water. Sections

were then stained with Hematoxylin and Eosin (H&E) solution (BA4025, Baso, Shanghai, China), Masson staining solution (BA4079, Baso, Shanghai, China) and Oil red O staining solution (BA4081, Baso, Shanghai, China). All sections were examined using a microscope (NIB910, Boshida, Shanghai, China).

EPCs Isolation and Culture

EPCs were isolated as previously described [17]. After euthanasia, the mice were immersed in 75% alcohol for 5 minutes. Then, under aseptic conditions, the femur was harvested and the surrounding muscle tissue was removed. The bone marrow tissue was flushed out with DMEM/F12 medium (iCell-0005, iCellbioscience, Shanghai, China) and passed through a 200-mesh stainless steel screen. The filtered cell suspension was washed with DMEM/F12, then resuspended in lymphocyte separation solution (DKW33-R0100, DAKEWE, Shenzhen, China), and centrifuged at 1500 rpm for 30 minutes. The resulting cloudy cell layer was collected with a pipette and cultured in DMEM/F12 medium. Cell morphology was observed under a microscope at 1, 2, 4, 8 and 14 days of culture.

Identification of EPCs

EPCs isolated from Control group were identified using immunofluorescence. Briefly, EPCs were seeded in 12-well plates, then fixed with 4% paraformaldehyde (BL539A, Biosharp, Beijing, China), permeabilized with 0.1% Triton X-100 (T88490, Acmec, China), blocked with 5% goat serum (BL736A, Biosharp, Beijing, China). Then, these cells were incubated overnight with anti-CD133 (AF5120, Affinity, Liyang, China), anti-CD34 (AF5149, Affinity, Liyang, China), anti-VEGFR2 antibodies (AF6281, Affinity, Liyang, China), and stained with secondary antibodies Goat Anti-Rabbit IgG (H+L) FITC-conjugated (S0008, Affinity, Liyang, China) and Goat Anti-Rabbit IgG (H+L) Fluor594-conjugated (S0006, Affinity, USA) in the following day. For acetylate low-density lipoprotein (ac-LDL) and ulex europaeus agglutinin-1 (UEA-1) uptake, EPCs were incubated with 20 μg/mL Dil-ac-LDL (MP6013-500UG, Maokang, Shanghai, China) for 4 hours and then incubated with 10 μg/mL FITC-UEA-I (MP6308-500UG, Maokang, Shanghai, China) for 1 hour. The nuclei were labeled with DAPI (BL120A, Biosharp, China). The results were observed under a fluorescence microscope (BZ-X800E, KEYENCE, Shanghai, China).

Transfection

STAT3 overexpression plasmid (oe-STAT3, G136744) were obtained from Youbio (Changsha, China) and their negative control (oe-NC, empty vector, V011817) were obtained from novopro (Shanghai, China). HPSE specific short hairpin RNA (shHPSE, 5′-CGGATGGATTACTTTCCAAAT-3′) and its NC (shNC, 5′-TTCTCCGAACGTGCACGTTTC-3′) were ordered from VectorBuilder (Guangzhou, China). One day before transfection, the cells were cultured at a density of approximately 5×10^5 cells per well in six-well plates. Opti-MEM Medium (31985062, ThermoFisher, Waltham, MA, USA) was used to dilute the transfection agents and plasmids. The plasmid-lipid complex was added to the six-well plates and thoroughly blended before incubation for 48 hours. Finally, quantitative reverse transcription polymerase chain reaction (qRT-PCR) was used to analyze the transfected cells.

Cell Grouping

The cellular experiments were divided into two parts. In the first part, cells isolated from the Model group were divided into four groups: Control, NGR1, NGR1+oe-NC and NGR1+oe-STAT3 groups. Except for the normal culture of cells in the Control group, the other three groups of cells were exposed to NGR1 (100 μg/mL) as previously described [18]. And cells in the latter two groups were transfected with oe-NC or oe-STAT3 before exposure to NGR1.

In the second part, cells were divided into four groups: oe-NC+shNC, oe-NC+shHPSE, oe-STAT3+shNC and oe-STAT3+shHPSE groups. EPCs were co-transfected with oe-NC/oe-STAT3 and shNC/shHPSE.

Cell Viability

The Cell Counting Kit-8 (CCK-8, PH1759, PHYGENE, Fuzhou, China) was used to assess cell viability. In 96-well plates, cells were injected and subsequently subjected to various treatments. The CCK-8 reagent was then added to the reaction well, followed by a two-hour incubation period at 37 °C. A microplate reader was used to measure the optical density (OD) value at 450 nm (HBS-ScanX, DeTiebio, Nanjing, China).

Colony Formation Assay

DMEM/F12 medium and 10% FBS were used to culture EPCs (1000 per well) for ten days. The cells were fixed with 4% paraformaldehyde before staining with crystal violet (BP-DL131, Sbjbio, Beijing, China). Colony formation was calculated by counting the relative number of colonies under an optical microscope.

Scratch Assay

To assess the migratory capacity of EPCs, a scratch assay was performed. In a nutshell, 5×10^5 cells were seeded into the 6-well plates and cultured until 90% confluence was reached. The EPCs were washed with Phosphate buffer saline (PBS, ms3560, Maokang, Shanghai, China) after the full medium was removed. Then, vertical lines were scratched onto the cells in each well using a pipette tip. The cells were rinsed three times with PBS to remove detached cells and debris, and serum-free medium was then poured into the plates. Images were captured at 0 and 48 hours using an inverted optical microscope (magnification:

Table 1. Antibodies used in this study.

Name	Catalog	Molecular weight	Dilution	Manufacturer
p-STAT3	ab32143	98 kDa	1/1000	abcam, Cambridge, UK
STAT3	ab68153	88 kDa	1/2000	abcam, Cambridge, UK
Heparanase	CY8458	70 kDa	1/1000	Abways, Shanghai, China
SDC-1	ab60199	32 kDa	1/2000	abcam, Cambridge, UK
GAPDH	ab8245	36 kDa	1/10,000	abcam, Cambridge, UK
Goat anti-Rabbit	ab205718	—	1/2000	abcam, Cambridge, UK
Goat anti-Mouse	ab205719	—	1/2000	abcam, Cambridge, UK

STAT3, Signal transducer and activator of transcription 3; SDC-1, syndecan-1; GAPDH, Glyceraldehyde-3-phosphate dehydrogenase.

100×), and cell migration rates were quantified with ImageJ (version 5.0; Bio-Rad, Herculaneum, CA, USA).

Tube Formation Assay

The Matrigel (356231, Corning, USA) was applied to each well of a 96-well plate and polymerized at 37 °C for 30 min. The 96-well plates were then filled with EPCs (1×10^4 cells/well), thoroughly mixed, and incubated for 8 hours at 37 °C with 5% CO_2. The relative tube length was examined using an inverted optical microscope and ImageJ software.

Western Blot Analysis

Proteins were extracted from EPCs using radio immunoprecipitation assay (RIPA) solution (MP1501, Maokang, Shanghai, China). Next, the relative protein concentration was quantified using a BCA kit (PMK0442, BIOPRIMACY, Wuhan, China). After being electrophoresed by SDS-PAGE (PH0331, PHYGENE, Fuzhou, China), the protein samples were transferred to the nitrocellulose membranes. Subsequently, the membranes were blocked with western blocking buffer (BL535A, Biosharp, Beijing, China) and incubated overnight at 4 °C with primary antibodies specific to the proteins of interest (Table 1). Then, the membranes were treated with the secondary antibodies (Table 1) and cultured with the ECL kit (MM0710, Maokang, Shanghai, China). GAPDH served as a loading control. After the membranes were exposed under the imaging system (JY04S-3, Beijing JUNYI Electrophoresis Co., Ltd., Beijing, China), the gray value of all protein bands was quantified by ImageJ.

Gene Expression Analysis

The total RNA was extracted from EPCs using TRIzol reagent (MF0403, Maokang, Shanghai, China), and reverse transcribed into cDNA using a reverse transcription kit (1708890, Maokang, Shanghai, China). The Real-Time PCR System (RTQ-960, Acon, Shenzhen, China) equipped with qPCR MasterMix (1725124, Maokang, Shanghai, China) was then used to conduct qPCR. The gene expression was normalized to Glyceraldehyde-3-phosphate dehydrogenase (Gapdh) using the $2^{-\Delta\Delta CT}$ method. Table 2 provided a list of the specific primers.

Table 2. Primers used in this study.

Genes	5′→ 3′
Stat3 (mouse) Forward	ACCAACGACCTGCAGCAATA
Stat3 (mouse) Reverse	TCCATGTCAAACGTGAGCGA
Hpse(mouse) Forward	CTGTCCAACACCTTTGCAGC
Hpse (mouse) Reverse	CACTCGGAGTTTGCTCCTGT
Gapdh (mouse) Forward	CCCTTAAGAGGGATGCTGCC
Gapdh (mouse) Reverse	ACTGTGCCGTTGAATTTGCC

Dual-Luciferase Reporter Assay (DLRL)

JASPAR (https://jaspar.genereg.net/) was adopted for prediction on the binding sites between HPSE and STAT3. The two sites with the highest relative prediction scores (Site 1: 0.89; Site 2: 0.90), both exceeding the stringent threshold of 0.85, were selected for functional validation. Based on the predicted sequences from JASPAR, luciferase reporter plasmids HPSE-WT (wild type) and HPSE-MUT (mutant type) were constracted using the pGL3 vector (E1751, Promega, Madison, WI, USA). Target cells were then co-transfected with the reporter plasmids, oe-STAT3 or oe-NC, and pRL vector (E2241, Promega, Madison, WI, USA). After transfection, the luciferase activity was measured using the DLRL system (E1910, Promega, Madison, WI, USA), with Renilla luciferase activity serving as an internal control.

Chromatin Immunoprecipitation (ChIP)

ChIP was performed using a ChIP detection kit (P2078, Beyotime, Shanghai, China). Cells were first exposed to 4% formaldehyde for 10 minutes to crosslink protein and DNA, followed by the addition of glycine to a final concentration of 125 mM for 5 minutes to quench the reaction. The residual cell precipitate was centrifuged, and it was then resuspended in the lysate. The DNA was divided into 250–350 kb using the ultrasonic procedure. Following purification, the samples were treated with A/G magnetic beads and either an anti-STAT3 antibody (12640, Cell Signaling Technology, Danvers, MA, USA) or an anti-IgG antibody (ab171870, Abcam, Cambridge, UK). Following elution and reversal of cross-links, the precipitated DNA was analyzed by qPCR.

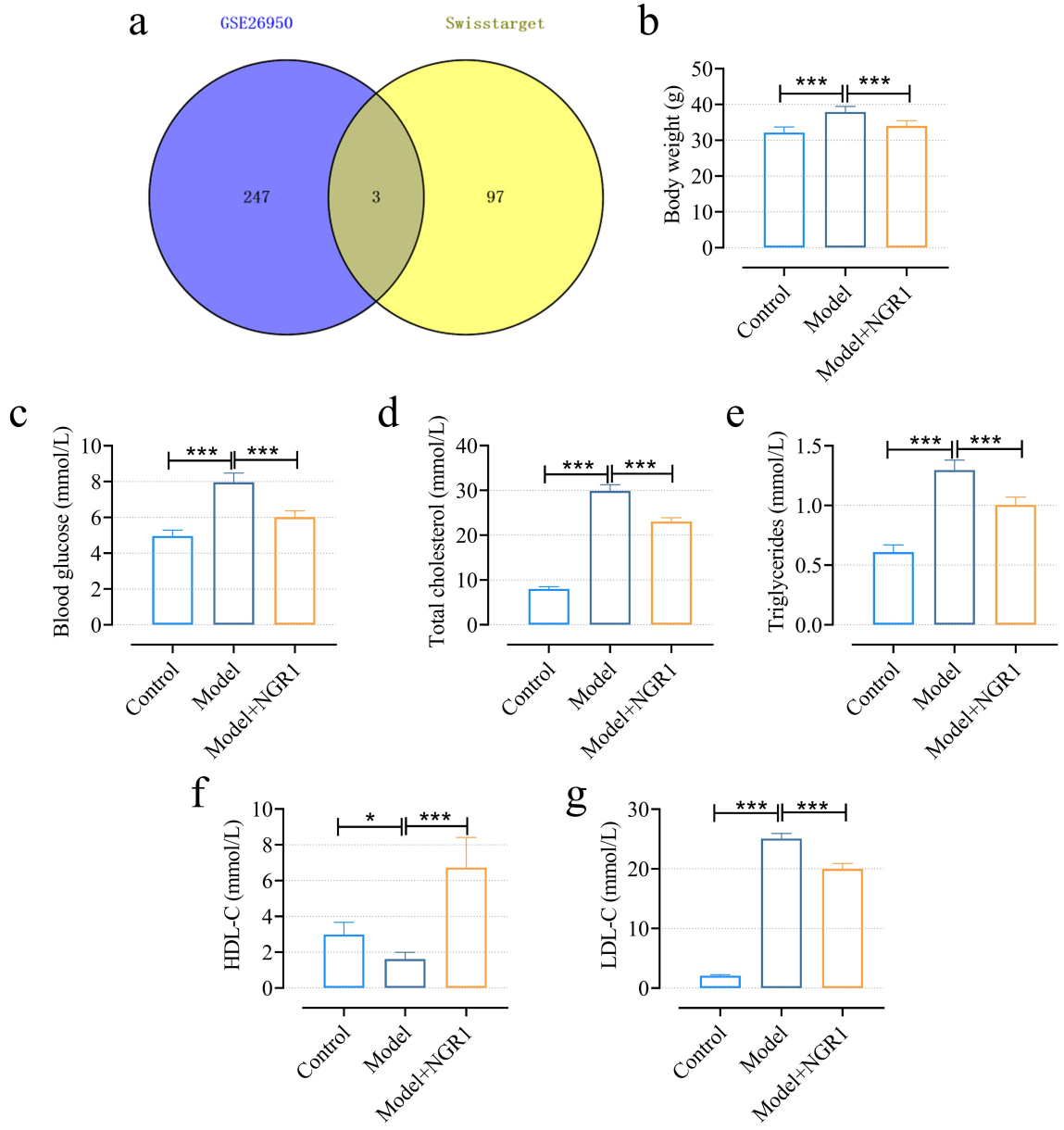

Fig. 1. Effects of NGR1 on AS model mice. ApoE$^{-/-}$ mice were exposed to Ang II to establish the AS model, and then they were treated with NGR1. (a) The dataset GSE26950 analyzed the differentially expressed genes in EPCs treated with IFN-α. Among them, there were 3 intersections with the NGR1 target predicted by Swisstargetprediction. (b) The body weight of mice. (c) The blood glucose was determined by a glucometer. (d–g) The lipid-related indexes (Total cholesterol, Triglycerides, HDL-C and LDL-C) were determined with corresponding kits. $^{*}p < 0.05$, $^{***}p < 0.001$. Quantified values were presented as mean $\pm$ standard deviation of three independent experiments (n = 3). NGR1, Notoginsenoside R1; Ang II, angiotensin II; AS, atherosclerosis; HDL-C, high-density lipoprotein cholesterol; LDL-C, Low-density Lipoprotein Cholesterol; ApoE$^{-/-}$, Apolipoprotein E-deficient.

Statistical Analyses

Graph Prism v8.0 (GraphPad software, San Diego, CA, USA) were employed to analyze the results. The data were represented as mean $\pm$ standard deviation. One-way analysis of variance was applied for the analysis of variance between multiple groups, followed by the Tukey post hoc test. $p < 0.05$ was considered statistically a significant difference.

Results

NGR1 Ameliorated Disturbances of Lipid Metabolism and Aortic Plaque in AS Mice

We firstly analyzed the differential gene (GSE26950) of IFN-α in the treatment of EPCs, and then crossed with the target of NGR1 predicted by Swisstargetprediction. HPSE has been demonstrated (Fig. 1a). To explore the ef-

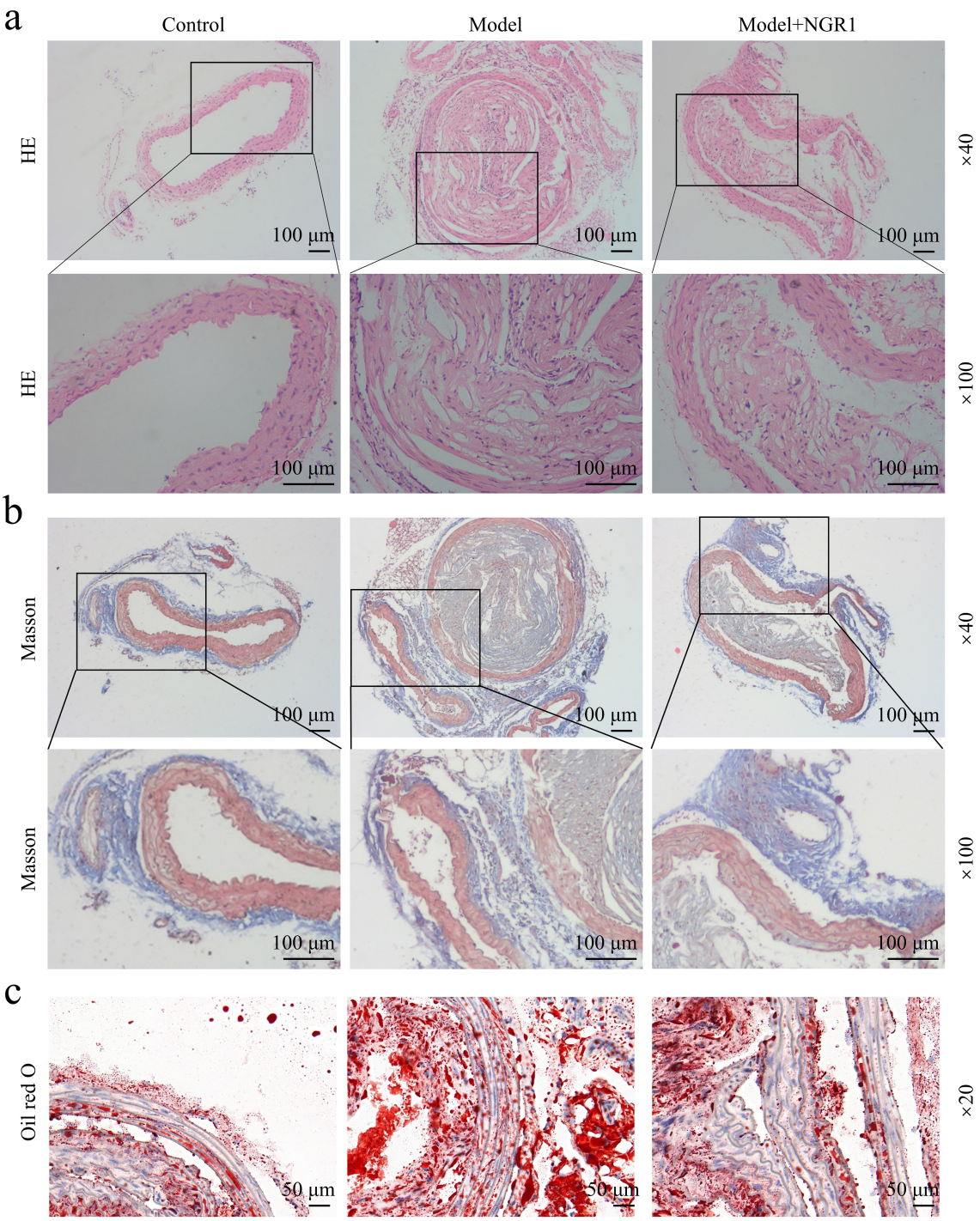

Fig. 2. Effects of NGR1 on AS model mice histopathological characteristics. (a–c) The histopathological characteristics were measured by H&E staining (a), Masson staining (b) and Oil red O staining (c) (magnification, 20×, 40×, 100×). Bar: 50 or 100 μm. H&E, Hematoxylin and eosin.

fect of NGR1 on AS, we evaluated the physiological parameters in AS mice with or without NGR1 treatment. Compared with the control group, the body weight (Fig. 1b), blood glucose (Fig. 1c), total cholesterol (Fig. 1d), triglycerides (Fig. 1e) and LDL-C (Fig. 1g) levels of mice in the model group were significantly increased ($p < 0.001$), while HDL-C (Fig. 1f) level of mice in the model group were significantly decreased ($p < 0.05$). However, under the intervention of NGR1, the levels of these indicators (except HDL-C) were decreased, while HDL-C levels were increased (Fig. 1a–f, $p < 0.001$). Subsequent histopathological analysis showed that aortic plaque necrosis, collagen fiber area reduction and lipid accumulation occurred in the model group (Fig. 2a–c). After treatment with NGR1,

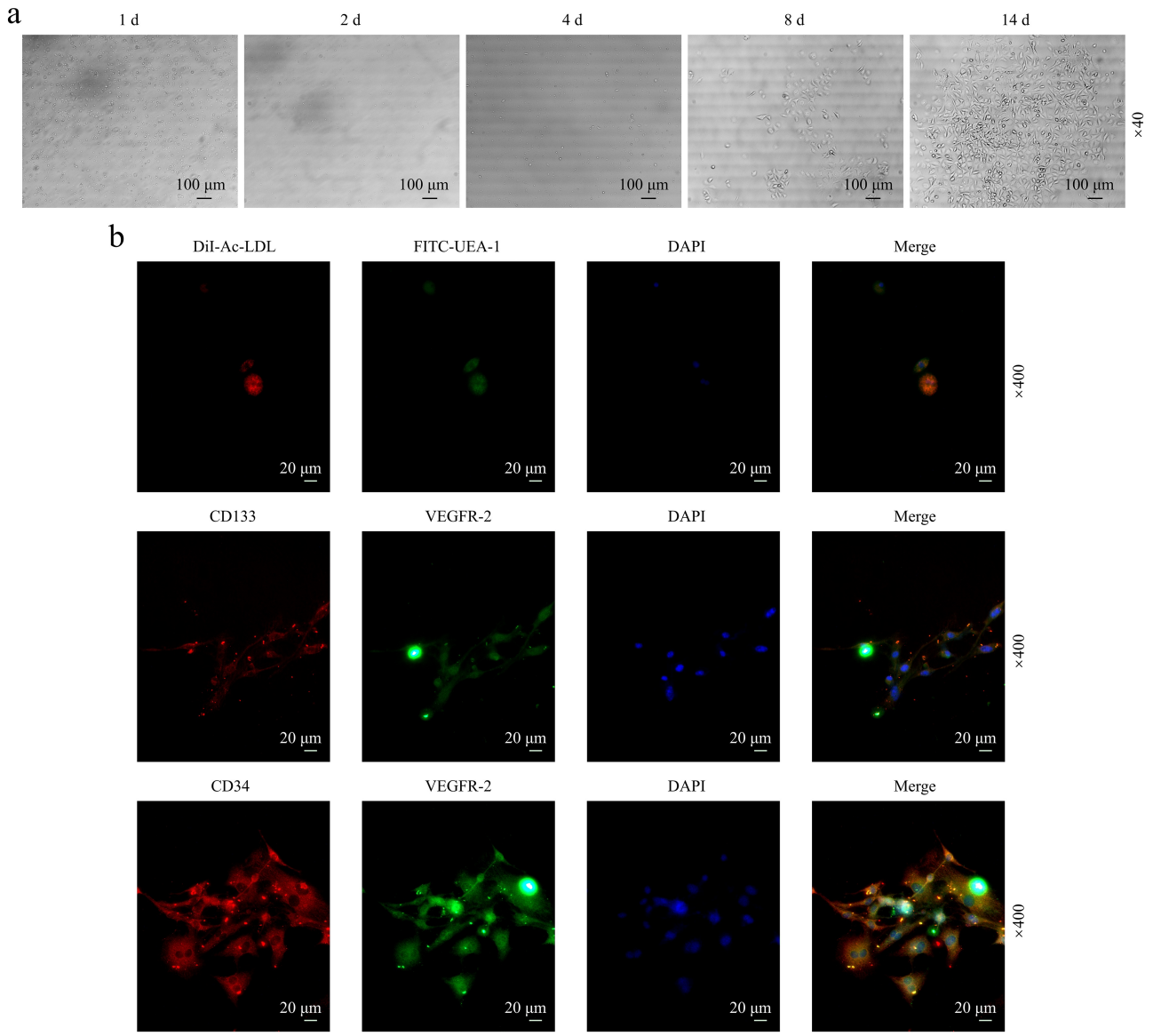

Fig. 3. Identification of EPCs. EPCs were extracted from the healthy control mice. (a) Cellular morphology was imaged under a microscope on Days 1, 2, 4, 8 and 14. (b) The Immunofluorescence assay was used to detect the EPCs (magnification, 400×). Bar: 20 μm. EPCs, endothelial progenitor cells.

the pathological lesions in the aforementioned model group were alleviated (Fig. 2a–c).

NGR1 Facilitated the Viability, Proliferation, Migration and Tube Formation of EPCs While Downregulating the Expression Levels of STAT3 and Heparanase

To investigate the effect of NGR1 on EPCs, EPCs were first isolated from healthy control mice to establish and validate our isolation protocol. As shown in Fig. 3a, these cells exhibited the typical cobblestone morphology of EPCs during culture. Immunofluorescence results showed that all cells we extracted expressed the EPCs markers CD133, CD34, and VEGFR2 (Fig. 3b). In addition, these cells exhibited uptake of Dil-Ac-LDL and binding to FITC-UEA-I, further indicating that their identity as EPCs (Fig. 3b). Then, we extracted EPCs from each group of mice for functional experiments. We found that the viability (Fig. 4a), cloning ability (Fig. 4b,d), migration ability (Fig. 4c,e) and angiogenesis ability (Fig. 5a,b) of EPCs derived from model mice were lower than those of EPCs derived from control mice ($p < 0.001$). However, EPCs derived from the model+NGR1 group were more potent than EPCs derived from the model mice in terms of viability, clonal ability, migration and angiogenesis ability (Fig. 4a–e, Fig. 5a,b, $p < 0.05$). Moreover, EPCs in the model group expressed p-STAT3, STAT3, and Heparanase, which were all reversed by NGR1 treatment (Fig. 5c–g, $p < 0.001$).

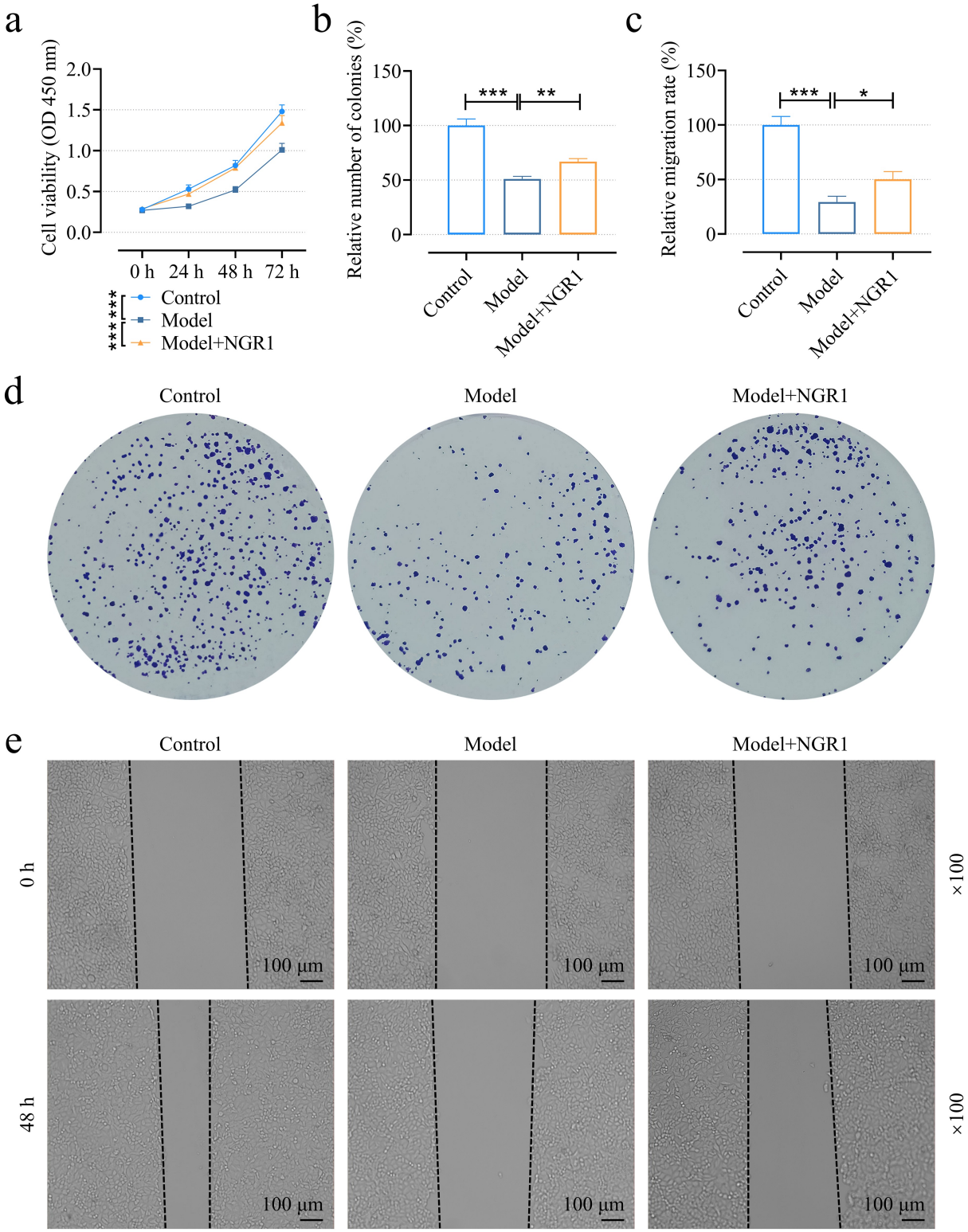

Fig. 4. NGR1 facilitated the viability, colon formation and migration of EPCs extracted from AS mice. EPCs were extracted from the bone marrow of the each group of mice. (a) The cell viability was determined by CCK-8. (b,d) The Relative number of colonies was examined by clone formation assay. (c,e) The Relative migration rate was determined by scratch assay (magnification, 100×). Bar: 100 μm. $^{*}p < 0.05$, $^{**}p < 0.01$, $^{***}p < 0.001$. Quantified values were presented as mean ± standard deviation of three independent experiments (n = 3). NGR1, Notoginsenoside R1; AS, atherosclerosis; EPCs, endothelial progenitor cells; CCK-8, Cell counting kit 8.

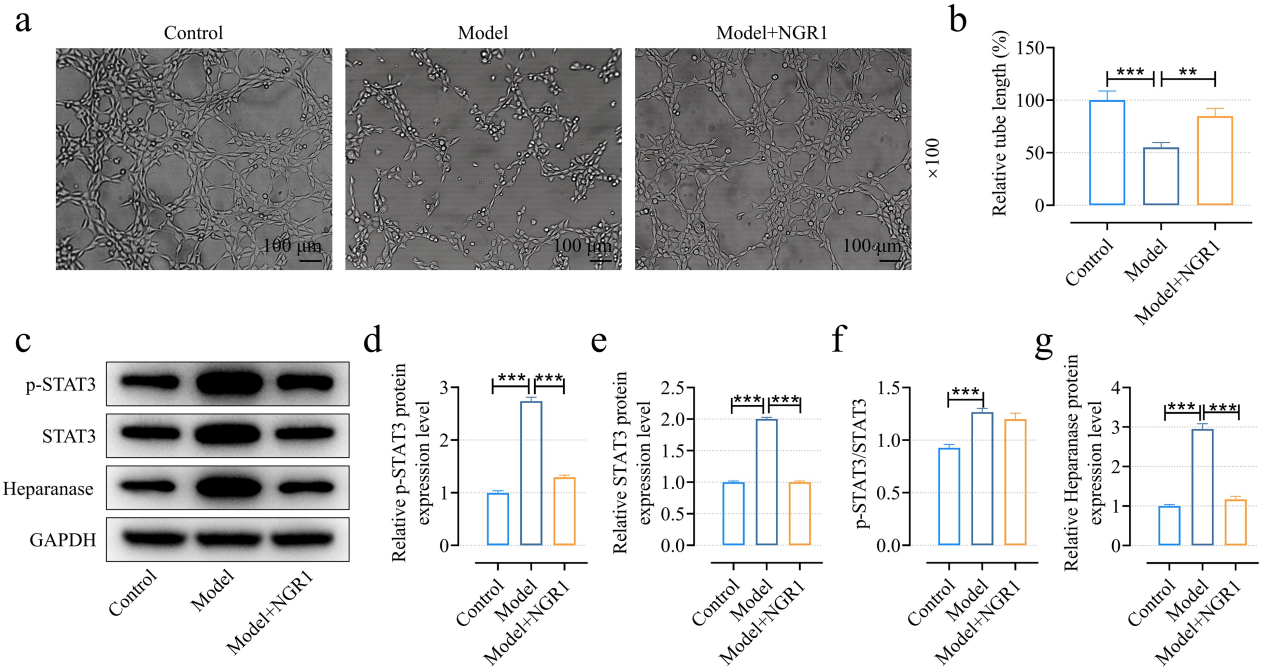

Fig. 5. Effect of NGR1 on tube formation and expression levels of STAT3 and Heparanase in EPCs extracted from AS mice. EPCs were extracted from the bone marrow of the each group of mice. (a,b) The relative tube length was determined by tube formation assay (magnification, 100×). Bar: 100 μm. (c–g) The expression levels of p-STAT3, STAT3 and Heparanase were determined by Western blotting. GAPDH was used as an internal control. $^{**}p < 0.01$, $^{***}p < 0.001$. Quantified values were presented as mean ± standard deviation of three independent experiments (n = 3). NGR1, Notoginsenoside R1; AS, atherosclerosis; EPCs, endothelial progenitor cells; GAPDH, Glyceraldehyde-3-phosphate dehydrogenase.

Oe-STAT3 Reversed the Effects of NGR1 on Viability, Proliferation, Migration and Tube Formation of EPCs As Well As the Expression Levels of Heparanase and Syndecan-1 (SDC-1)

To further investigate whether the therapeutic effect of NGR1 was associated with STAT3, EPCs extracted from Model mice were transfected and induced *in vitro* by NGR1. Oe-STAT3 successfully promoted the expression of *STAT3* in EPCs (Fig. 6a, $p < 0.001$). Under the induction of NGR1, the viability (Fig. 6b), migration ability (Fig. 6c,e), cloning ability (Fig. 6d,f) and angiogenesis ability (Fig. 7a,b) of EPCs were increased ($p < 0.01$), while these effects were all reversed by oe-STAT3 (Fig. 5b–f, Fig. 6a,b, $p < 0.05$). Furthermore, NGR1 resulted in the decrease of Heparanase expression and the increase of SDC-1 expression in EPCs, but the transfection of oe-STAT3 reversed these effects (Fig. 7c–e, $p < 0.001$).

STAT3 Activated HPSE Transcription

To investigate whether STAT3 could regulate the transcription of HPSE, we obtained the DNA motif of STAT3 through JASPAR (Fig. 7f). Then, we found two high-confidence binding sites for STAT3 (designated Site 1 and Site 2, Fig. 7g) within the HPSE promoter, which were selected for experimental validation based on their top prediction scores. DLRL demonstrated that oe-STAT3 promotes the luciferase activity of HPSE-WT, which was attenuated by either MUT-1 or MUT-2 (Fig. 7h, $p < 0.01$). For the MUT group with simultaneous mutation at both sites, the luciferase activity was not affected by oe-STAT3 (Fig. 7h). In addition, the ChIP experiment also verified the binding of STAT3 to the HPSE promoter (Fig. 7i, $p < 0.001$).

STAT3 Regulated the Viability, Proliferation, Migration and Tube Formation of EPCs As Well As the Expression Levels of SDC-1 by Upregulating HPSE

We silenced *HPSE* in EPCs to determine the causal role of HPSE and STAT3 in EPCs (Fig. 8a, $p < 0.001$). Notably, compared with the control group, higher vitality (Fig. 8b), migration ability (Fig. 8c,e), cloning ability (Fig. 8d,f), angiogenesis ability (Fig. 9a,b) and more SDC-1 expression (Fig. 9c,d) were observed in EPCs transfected with shHPSE ($p < 0.001$). On the contrary, oe-STAT3 decreased migration ability, cloning ability and angiogenesis ability, and down-regulated SDC-1 in EPCs (Fig. 8c–f, Fig. 9a–d, $p < 0.001$). However, the effects of both shHPSE and oe-STAT3 on EPCs were neutralized by the co-transfection of shHPSE and oe-STAT3 (Fig. 8c–f, Fig. 9a–d, $p < 0.001$).

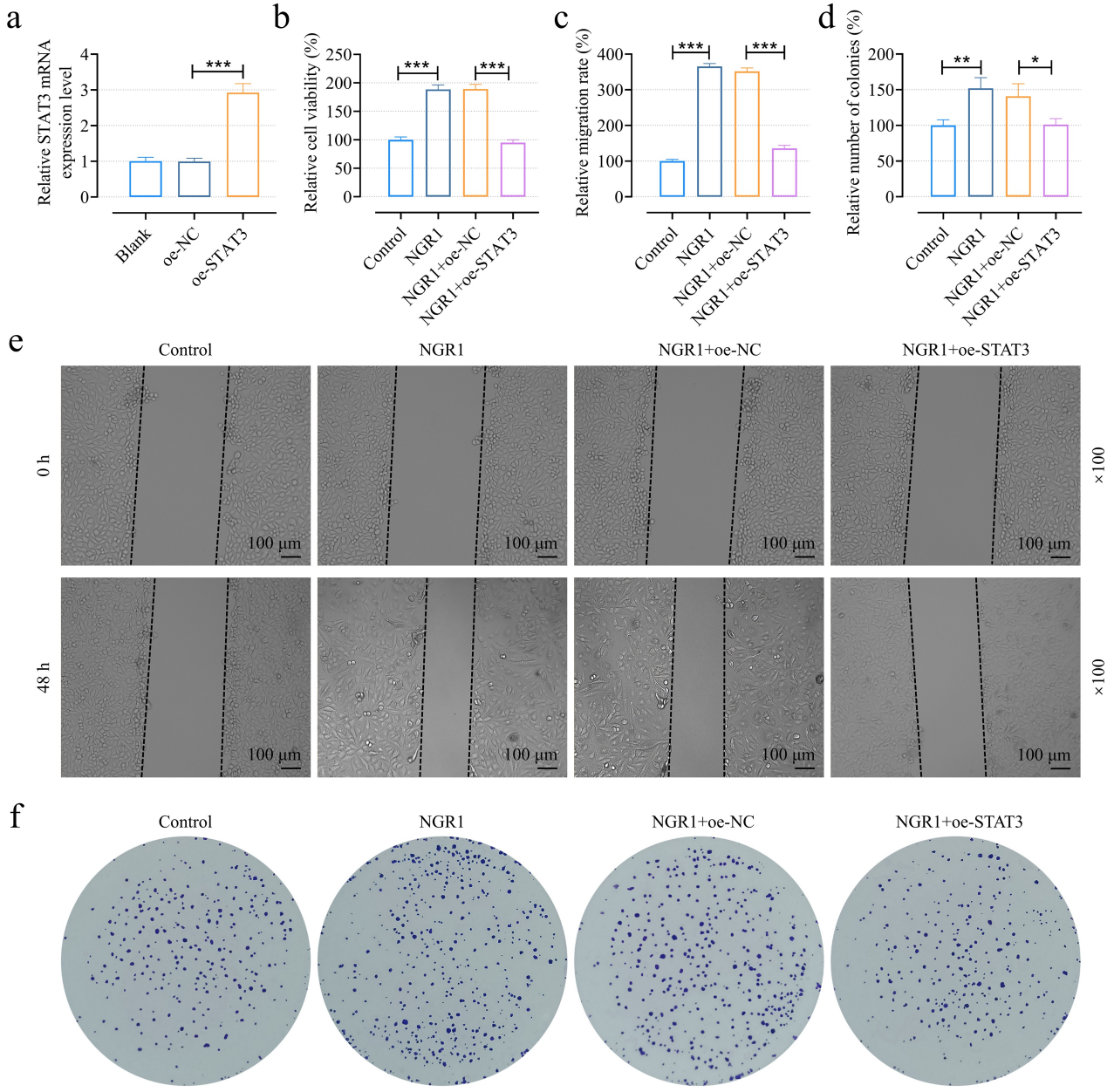

Fig. 6. STAT3 overexpression reversed the effects of NGR1 on viability, colon formation and migration of EPCs separated from AS mice. (a) The transfection efficiency of *STAT3* overexpression plasmid was determined by qRT-PCR. *GAPDH* was used as an internal control. For (b–f), EPCs separated from the bone marrow of the AS mice were transfected with oe-NC/STAT3 overexpression plasmid and then treated with NGR1 (100 μg/mL). (b) The cell viability was determined by CCK-8. (c,e) The relative migration rate was determined using scratch assay (magnification, 100×). Bar: 100 μm. (d,f) The relative number of colonies was examined by clone formation assay. $^{*}p < 0.05$, $^{**}p < 0.01$, $^{***}p < 0.001$. Quantified values were presented as mean ± standard deviation of three independent experiments (n = 3). NGR1, Notoginsenoside R1; AS, atherosclerosis; EPCs, endothelial progenitor cells; CCK-8, cell counting kit-8; GAPDH, Glyceraldehyde-3-phosphate dehydrogenase; qRT-PCR, quantitative real-time polymerase chain reaction.

Discussion

EPCs play a beneficial role in vascular repair and the treatment of AS. However, the number of EPCs in AS environment decreases, and the dysfunction limits the therapeutic effect of EPCs. Here, we report the improvement of EPCs' function by NGR1 and the underlying mechanisms.

We first evaluated the improvement of biochemical parameters and pathological damage of aortic tissue in AS mice by NGR1. The pathogenesis of AS is related to lipid accumulation. Increased expression of total cholesterol, triglycerides and LDL-C has been reported in patients with AS or in animal models of AS [19]. There is convincing evidence that lowering total cholesterol, triglyc-

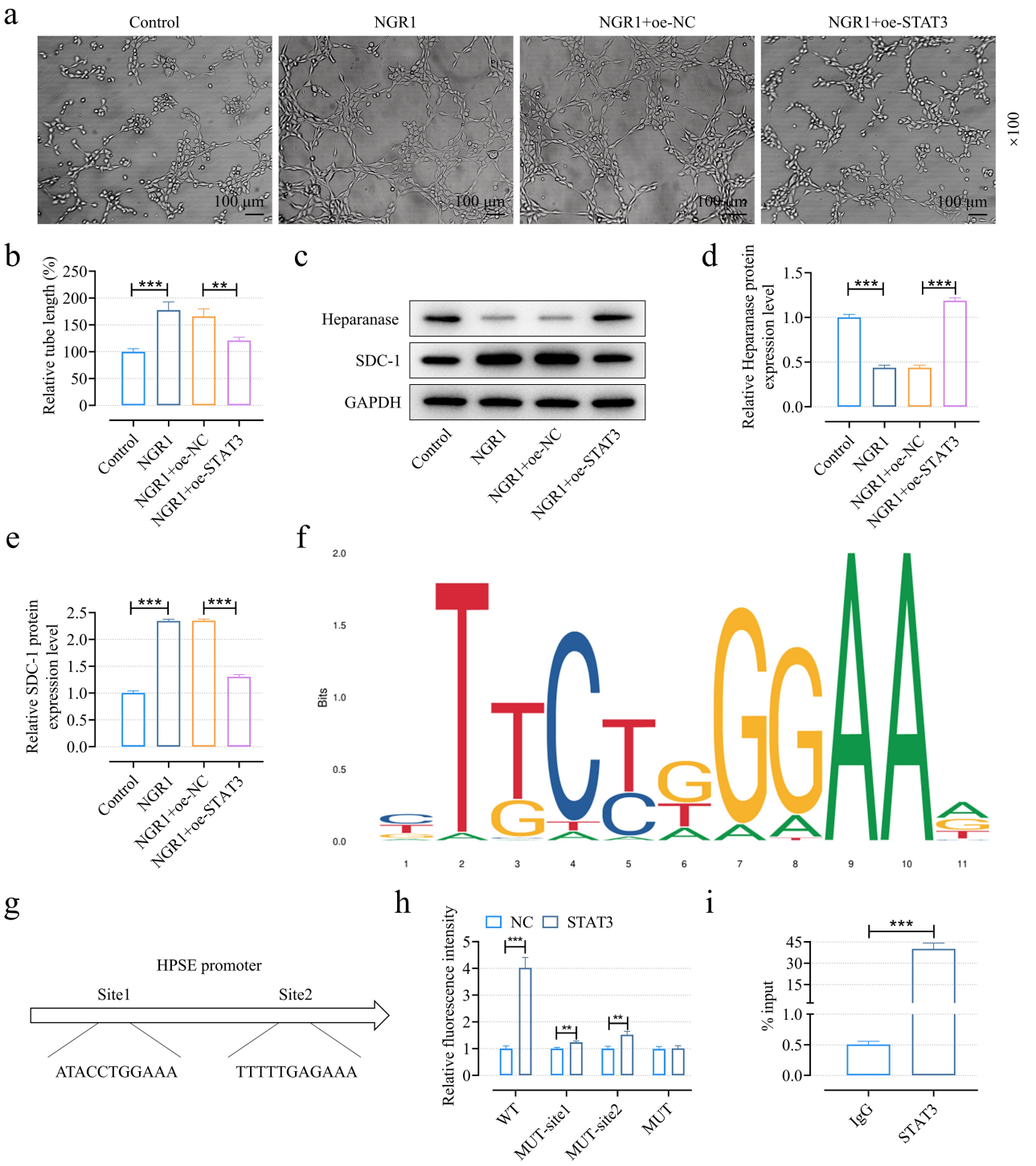

Fig. 7. Effects of STAT3 and NGR1 on tube formation and expression levels of Heparanase, and SDC-1 in EPCs and STAT3 activates HPSE transcription. EPCs extracted from the bone marrow of the AS mice were transfected with oe-NC/STAT3 overexpression plasmid and then treated with NGR1 (100 μg/mL). (a,b) The relative tube length was determined by tube formation assay (magnification, 100×). Bar: 100 μm. (c–e) The expression levels of Heparanase and SDC-1 were determined by Western blotting. GAPDH was used as an internal control. (f,g) JASPAR analysis of the binding site between STAT3 and HPSE. (h) A dual luciferase reporter gene assay was used to detect the binding of STAT3 and HPSE. (i) The combination of STAT3 and HPSE was detected using ChIP. $^{**}p < 0.01$, $^{***}p < 0.001$. Quantified values were presented as mean ± standard deviation of three independent experiments (n = 3). NGR1, Notoginsenoside R1; AS, atherosclerosis; EPCs, endothelial progenitor cells; ChIP, Chromatin immunoprecipitation; GAPDH, Glyceraldehyde-3-phosphate dehydrogenase; SDC-1, syndecan-1.

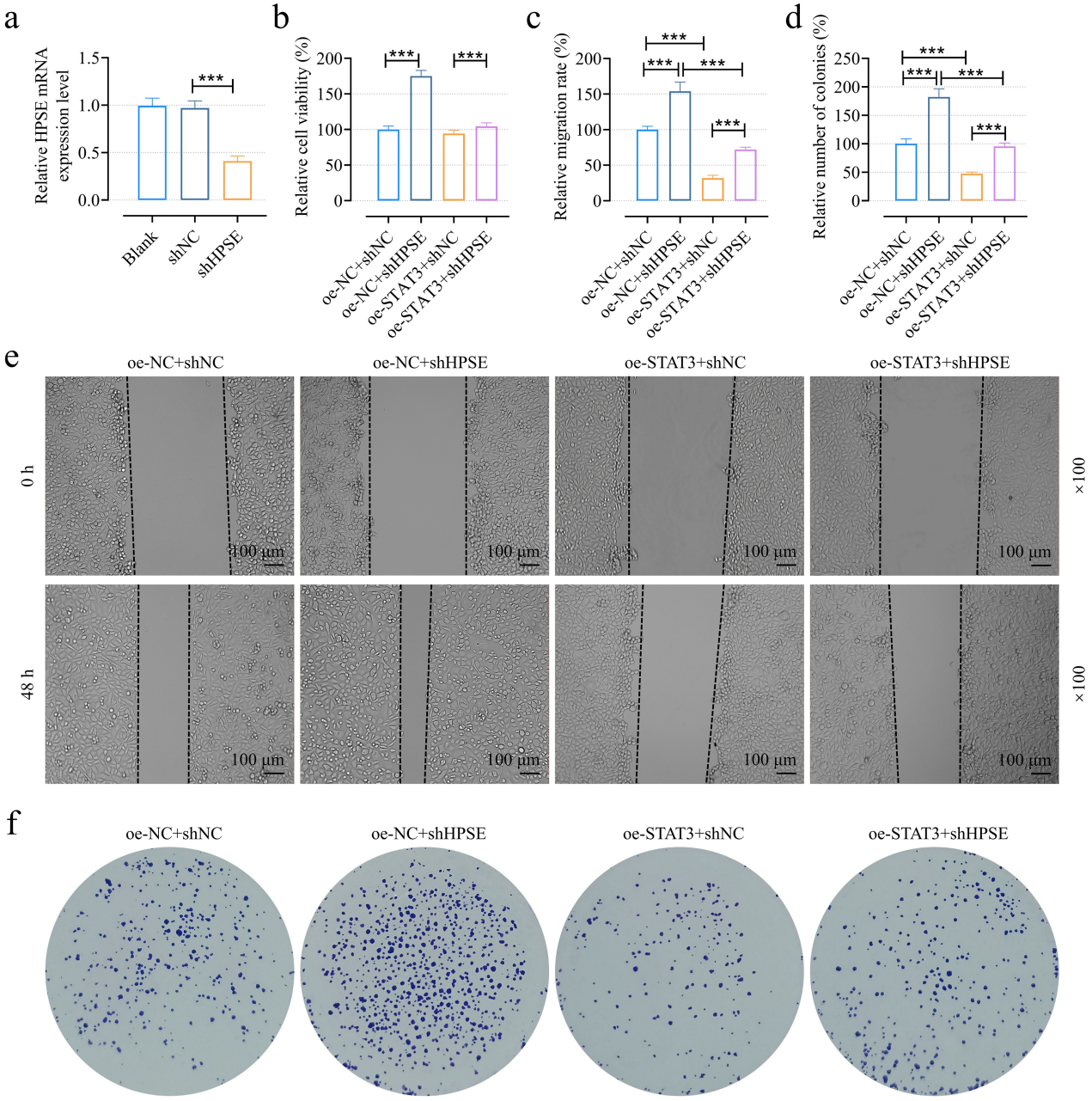

Fig. 8. Effects of shHPSE and STAT3 overexpression on viability, colon formation and migration in EPCs extracted from AS mice. (a) The transfection efficiency of shHPSE was determined by qRT-PCR. *GAPDH* was used as an internal control. For (b–f), EPCs extracted from the bone marrow of the AS mice were transfected with oe-NC/STAT3 overexpression plasmid and shNC/shHPSE. (b) The cell viability was determined by CCK-8. (c,e) The relative migration rate was determined by scratch assay (magnification, 100×). Bar: 100 μm. (d,f) The relative number of colonies was examined using clone formation assay. $^{***}p < 0.001$. Quantified values were presented as mean ± standard deviation of three independent experiments (n = 3). AS, atherosclerosis; EPCs, endothelial progenitor cells; CCK-8, cell counting kit-8; GAPDH, Glyceraldehyde-3-phosphate dehydrogenase; qRT-PCR, quantitative real-time polymerase chain reaction.

erides, and LDL-C can reduce AS-related cardiovascular events, while increasing HDL-C concentrations may play a role in the prevention of AS [20]. Herein, we reported that NGR1 could reduce blood glucose, total cholesterol, triglycerides, and LDL-C but increase HDL-C content in AS mice, which was also consistent with the results of the previous study [21]. In addition, histopathological analysis showed that NGR1 reduced the lipid accumulation in aorta and increased the area of collagen fibers, which was consistent with the previously reported results that NGR1 combined with geniposide improved the disorder of aortic plaque in AS mice [19].

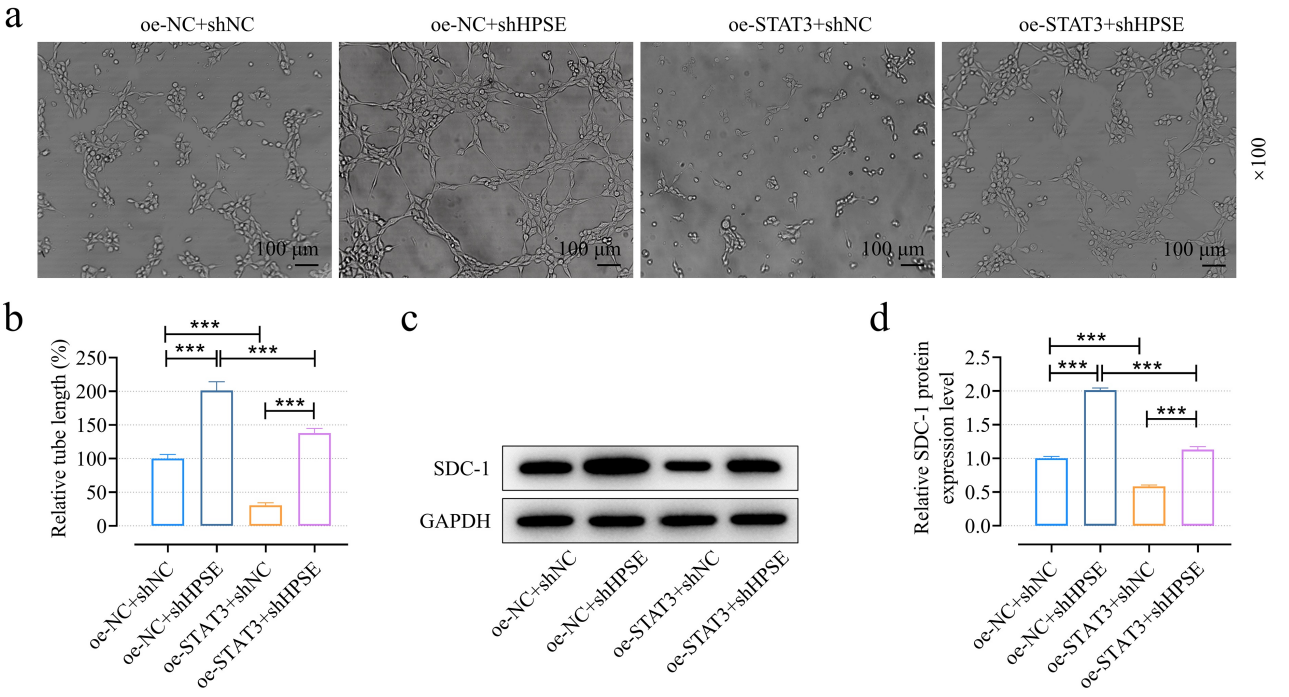

Fig. 9. Effects of shHPSE and STAT3 overexpression on tube formation and expression of SDC-1 in EPCs extracted from AS mice. EPCs extracted from the bone marrow of the AS mice were transfected with oe-NC/STAT3 overexpression plasmid and shNC/shHPSE. (a,b) The relative tube length was determined by tube formation assay (magnification, 100×). Bar: 100 μm. (c,d) The expression of SDC-1 were determined by Western blotting. GAPDH was used as an internal control. $^{***}p < 0.001$. Quantified values were presented as mean ± standard deviation of three independent experiments (n = 3). AS, atherosclerosis; EPCs, endothelial progenitor cells; GAPDH, Glyceraldehyde-3-phosphate dehydrogenase; SDC-1, syndecan-1.

To investigate the regulatory effect of NGR1 on EPCs, EPCs were extracted from mice. At present, the characterization methods of EPCs are not unified, and we identified EPCs using a dual approach involving the identification of EPCs' surface markers and the uptake of UEA-1 and acLDL by EPCs [2]. The endothelial repair function of EPCs depends on their migration from the initial part to the injured part, and then enhances angiogenesis by releasing cytokines and differentiating into an endothelial phenotype. However, EPCs in the AS environment showed impaired migration, proliferation, and angiogenesis abilities [17]. Accumulating evidence indicates that Panax notoginseng saponins have the ability to promote the proliferation, migration and angiogenesis of EPCs [7,22]. Consistently, our results indicate that NGR1, the main component of Panax notoginseng saponins, also improves the EPCs' function.

Next, our research focuses on the molecular mechanisms. In our study, STAT3 and Heparanase were upregulated in the AS mouse model, which was inhibited by NGR1. Accumulating evidence demonstrates that STAT3 translocates to the nucleus, binds to specific sequences on target gene promoters, and induces transcription of target genes (such as adhesion molecules), thus aggravating endothelial dysfunction and promoting the development of AS [14]. Crucially, our study identified that HPSE is a direct transcriptional target of STAT3. This establishes a primary link where STAT3 activation in dysfunctional EPCs drives HPSE expression. The HPSE expression has increased in patients with AS [23], and studies by Rabia Shekh Muhammad *et al.* [24] have shown that inhibition of HPSE can improve lipid accumulation in AS mice and alleviate AS development.

The existing research has demonstrated the inhibitory effect of NGR1 on STAT3 [25], but the inhibitory effect of NGR1 on HPSE remains unexplored. Importantly, STAT3 overexpression reversed the therapeutic effects of NGR1 on EPCs and concurrently downregulated SDC-1, whereas shHPSE rescued the STAT3-induced functional impairments and SDC-1 loss. SDC-1, a key component of the endothelial glycocalyx located at the top of endothelial cells, plays a role in regulating the permeability of endothelial cell barrier [26]. The shedding of glycocalyx has been proven to impair endothelial function [27]. Of note, HPSE regulates the biological behavior of endothelial cells by regulating the expression of SDC-1 [28,29]. Therefore, NGR1 may alleviate EPCs' dysfunction by regulating the STAT3-HPSE-SDC-1 axis, in which STAT3-driven HPSE transcription leads to SDC-1 ectodomain shedding, glycocalyx damage, and ultimately contributes to the observed

EPC dysfunction, including impaired migration, proliferation, and tube formation. This reveals a novel mechanistic pathway underlying NGR1's therapeutic effect in atherosclerosis.

Conclusion

In this study, we focused on the important role of EPCs in the pathogenesis of AS and revealed that NGR1 could improve EPCs' function via regulating the STAT3/HPSE axis, which might provide a new strategy for the treatment and prevention of AS.

Availability of Data and Materials

The analyzed data sets generated during the study are available from the corresponding author on reasonable request.

Author Contributions

FF designed the research study, performed the research, collected and analyzed the data. FF has been involved in drafting the manuscript and has been involved in revising it critically for important intellectual content. FF gives final approval of the version to be published. FF has participated sufficiently in the work to take public responsibility for appropriate portions of the content and agreed to be accountable for all aspects of the work in ensuring that questions related to its accuracy or integrity.

Ethics Approval and Consent to Participate

All animal-related experimental protocols were approved by Ethics Committee of Shaoxing People's Hospital for Experimental Animals Welfare (2022Z015).

Acknowledgment

Not applicable.

Funding

This research was funded by The Zhejiang Provincial Medical and Health Science and Technology Plan (grant number: 2022KY1286); The Zhejiang Provincial Traditional Chinese Medicine Science and Technology Plan Project (grant number: 2023ZL730); Shaoxing Science and Technology Plan Project (grant number: 2022A14017).

Conflict of Interest

The author declares no conflict of interest.

References

[1] Altabas V, Biloš LSK. The Role of Endothelial Progenitor Cells in Atherosclerosis and Impact of Anti-Lipemic Treatments on Endothelial Repair. International Journal of Molecular Sciences. 2022; 23: 2663. https://doi.org/10.3390/ijms23052663.

[2] Du F, Zhou J, Gong R, Huang X, Pansuria M, Virtue A, *et al*. Endothelial progenitor cells in atherosclerosis. Frontiers in Bioscience (Landmark Edition). 2012; 17: 2327–2349. https://doi.org/10.2741/4055.

[3] Pelliccia F, Zimarino M, De Luca G, Viceconte N, Tanzilli G, De Caterina R. Endothelial Progenitor Cells in Coronary Artery Disease: From Bench to Bedside. Stem Cells Translational Medicine. 2022; 11: 451–460. https://doi.org/10.1093/stcltm/szac010.

[4] Ding X, Xiang W, He X. IFN-I Mediates Dysfunction of Endothelial Progenitor Cells in Atherosclerosis of Systemic Lupus Erythematosus. Frontiers in Immunology. 2020; 11: 581385. https://doi.org/10.3389/fimmu.2020.581385.

[5] Mugale MN, Dev K, More BS, Mishra VS, Washimkar KR, Singh K, *et al*. A Comprehensive Review on Preclinical Safety and Toxicity of Medicinal Plants. Clinical Complementary Medicine and Pharmacology. 2024; 4: 100129. https://doi.org/10.1016/j.ccmp.2024.100129.

[6] Liu H, Zhu L, Chen L, Li L. Therapeutic potential of traditional Chinese medicine in atherosclerosis: A review. Phytotherapy Research: PTR. 2022; 36: 4080–4100. https://doi.org/10.1002/ptr.7590.

[7] Zhu P, Jiang W, He S, Zhang T, Liao F, Liu D, *et al*. Panax notoginseng saponins promote endothelial progenitor cell angiogenesis via the Wnt/β-catenin pathway. BMC Complementary Medicine and Therapies. 2021; 21: 53. https://doi.org/10.1186/s12906-021-03219-z.

[8] Chen W, Dang Y, Zhu C. Simultaneous determination of three major bioactive saponins of Panax notoginseng using liquid chromatography-tandem mass spectrometry and a pharmacokinetic study. Chinese Medicine. 2010; 5: 12. https://doi.org/10.1186/1749-8546-5-12.

[9] Liu H, Yang J, Yang W, Hu S, Wu Y, Zhao B, *et al*. Focus on Notoginsenoside R1 in Metabolism and Prevention Against Human Diseases. Drug Design, Development and Therapy. 2020; 14: 551–565. https://doi.org/10.2147/DDDT.S240511.

[10] Zhang L, Li Y, Ma X, Liu J, Wang X, Zhang L, *et al*. Ginsenoside Rg1-Notoginsenoside R1-Protocatechuic Aldehyde Reduces Atherosclerosis and Attenuates Low-Shear Stress-Induced Vascular Endothelial Cell Dysfunction. Frontiers in Pharmacology. 2021; 11: 588259. https://doi.org/10.3389/fphar.2020.588259.

[11] Ilhan F, Kalkanli ST. Atherosclerosis and the role of immune cells. World Journal of Clinical Cases. 2015; 3: 345–352. https://doi.org/10.12998/wjcc.v3.i4.345.

[12] Daina A, Michielin O, Zoete V. SwissTargetPrediction: updated data and new features for efficient prediction of protein targets of small molecules. Nucleic Acids Research. 2019; 47: W357–W364. https://doi.org/10.1093/nar/gkz382.

[13] Nguyen TK, Paone S, Chan E, Poon IKH, Baxter AA, Thomas SR, *et al*. Heparanase: A Novel Therapeutic Target for the Treatment of Atherosclerosis. Cells. 2022; 11: 3198. https://doi.org/10.3390/cells11203198.

[14] Chen Q, Lv J, Yang W, Xu B, Wang Z, Yu Z, *et al*. Targeted inhibition of STAT3 as a potential treatment strategy for atherosclerosis. Theranostics. 2019; 9: 6424–6442. https://doi.org/10.7150/thno.35528.

[15] Castro-Mondragon JA, Riudavets-Puig R, Rauluseviciute I, Lemma RB, Turchi L, Blanc-Mathieu R, *et al*. JASPAR 2022: the 9th release of the open-access database of transcription factor binding profiles. Nucleic Acids Research. 2022; 50: D165–D173. https://doi.org/10.1093/nar/gkab1113.

[16] Liu YS, Yang Q, Li S, Luo L, Liu HY, Li XY, *et al*. Luteolin attenuates angiotensin II induced renal damage in apolipoprotein E deficient mice. Molecular Medicine Reports. 2021; 23: 157. https://doi.org/10.3892/mmr.2020.11796.

[17] Li Y, Cui W, Song B, Ye X, Li Z, Lu C. Autophagy-Sirtuin1(SIRT1) Alleviated the Coronary Atherosclerosis (AS)in Mice through Regulating the Proliferation and Migration of Endothelial Progenitor Cells (EPCs) via wnt/β-catenin/GSK3β Signaling Pathway. The Journal of Nutrition, Health & Aging. 2022; 26: 297–306. https://doi.org/10.1007/s12603-022-1750-7.

[18] Zhang WJ, Wojta J, Binder BR. Notoginsenoside R1 counteracts endotoxin-induced activation of endothelial cells in vitro and endotoxin-induced lethality in mice in vivo. Arteriosclerosis, Thrombosis, and Vascular Biology. 1997; 17: 465–474. https://doi.org/10.1161/01.atv.17.3.465.

[19] Liu X, Xu Y, Cheng S, Zhou X, Zhou F, He P, *et al*. Geniposide Combined With Notoginsenoside R1 Attenuates Inflammation and Apoptosis in Atherosclerosis *via* the AMPK/mTOR/Nrf2 Signaling Pathway. Frontiers in Pharmacology. 2021; 12: 687394. https://doi.org/10.3389/fphar.2021.687394.

[20] Lu H, Daugherty A. Atherosclerosis. Arteriosclerosis, Thrombosis, and Vascular Biology. 2015; 35: 485–491. https://doi.org/10.1161/ATVBAHA.115.305380.

[21] Jia C, Xiong M, Wang P, Cui J, Du X, Yang Q, *et al*. Notoginsenoside R1 attenuates atherosclerotic lesions in ApoE deficient mouse model. PloS One. 2014; 9: e99849. https://doi.org/10.1371/journal.pone.0099849.

[22] Liu Y, Hao F, Zhang H, Cao D, Lu X, Li X. Panax notoginseng saponins promote endothelial progenitor cell mobilization and attenuate atherosclerotic lesions in apolipoprotein E knockout mice. Cellular Physiology and Biochemistry: International Journal of Experimental Cellular Physiology, Biochemistry, and Pharmacology. 2013; 32: 814–826. https://doi.org/10.1159/000354484.

[23] Osterholm C, Folkersen L, Lengquist M, Pontén F, Renné T, Li J, *et al*. Increased expression of heparanase in symptomatic carotid atherosclerosis. Atherosclerosis. 2013; 226: 67–73. https://doi.org/10.1016/j.atherosclerosis.2012.09.030.

[24] Muhammad RS, Abu-Saleh N, Kinaneh S, Agbaria M, Sabo E, Grajeda-Iglesias C, *et al*. Heparanase inhibition attenuates atherosclerosis progression and liver steatosis in E_0 mice. Atherosclerosis. 2018; 276: 155–162. https://doi.org/10.1016/j.atherosclerosis.2018.07.026.

[25] Lu M, Xie K, Lu X, Lu L, Shi Y, Tang Y. Notoginsenoside R1 counteracts mesenchymal stem cell-evoked oncogenesis and doxorubicin resistance in osteosarcoma cells by blocking IL-6 secretion-induced JAK2/STAT3 signaling. Investigational New Drugs. 2021; 39: 416–425. https://doi.org/10.1007/s10637-020-01027-9.

[26] Dogné S, Flamion B. Endothelial Glycocalyx Impairment in Disease: Focus on Hyaluronan Shedding. The American Journal of Pathology. 2020; 190: 768–780. https://doi.org/10.1016/j.ajpath.2019.11.016.

[27] Edwards N, Langford-Smith AWW, Wilkinson FL, Alexander MY. Endothelial Progenitor Cells: New Targets for Therapeutics for Inflammatory Conditions With High Cardiovascular Risk. Frontiers in Medicine. 2018; 5: 200. https://doi.org/10.3389/fmed.2018.00200.

[28] Chen X, Cheng B, Dai D, Wu Y, Feng Z, Tong C, *et al*. Heparanase induces necroptosis of microvascular endothelial cells to promote the metastasis of hepatocellular carcinoma. Cell Death Discovery. 2021; 7: 33. https://doi.org/10.1038/s41420-021-00411-5.

[29] Yu S, Lv H, Zhang H, Jiang Y, Hong Y, Xia R, *et al*. Heparanase-1-induced shedding of heparan sulfate from syndecan-1 in hepatocarcinoma cell facilitates lymphatic endothelial cell proliferation via VEGF-C/ERK pathway. Biochemical and Biophysical Research Communications. 2017; 485: 432–439. https://doi.org/10.1016/j.bbrc.2017.02.060.